

Control the qubit-qubit coupling with double superconducting resonators

Hui Wang,^{1,2,*} Rui Wang,³ Daichi Sugiyama,¹ and J.S. Tsai^{1,2}

¹Department of Physics, Graduate School of Science,
Tokyo University of Science, Shinjuku-ku, Tokyo, Japan

²RIKEN Center for Quantum Computing (RQC), Wako-shi, Saitama, Japan

³Fujitsu Limited, Nakahara-ku, Kawasaki, Kanagawa 211-8588, Japan

(Dated: February 13, 2026)

We experimentally studied the switching off processes in the double-resonator coupler superconducting quantum circuit. In both frequency and time-domain, we observed the variation of qubit-qubit effective coupling by tuning qubits' frequencies. According to the measurement results, by just shifting qubits' frequencies smaller than 50 MHz, the effective qubit-qubit coupling strength can be tuned from switching off point to two qubit gate point (effective coupling larger than 5 MHz) in double-resonator superconducting quantum circuit. The double-resonator coupler superconducting quantum circuit has the advantage of simple fabrications, introducing less flux noises, reducing occupancy of dilution refrigerator cables, which might supply a promising platform for future large-scale superconducting quantum processors.

I. INTRODUCTION

The tunable coupler has the advantage of switchable interaction, fast two-qubit gates, reduced residual ZZ and idling errors, and cleaner scaling to many qubits, which becomes indispensable devices in the multi-qubit superconducting quantum chip[1–8]. The transmon coupler is the mainstream in the current large-size superconducting quantum chip and realizing the quantum supremacy and initial quantum errors [5–11].

As shown by previous theoretically and experimentally research, the superconducting resonator can also function as a tunable coupler for the superconducting qubits[12–18]. According to recent theoretical work [18], the double-resonator coupler can switch off the qubit-qubit effective coupling and their static ZZ coupling, and the double-resonator coupler have special advantage of simple fabrications, small frequency tuning ranges, less flux noise, and without occupying a dilution refrigerator cables.

In this article, we experimentally studied the switching off processes in the double-resonator coupler superconducting quantum circuit. In both frequency and time-domain, we measured the variation of qubit-qubit coupling strength by tuning frequency differences of qubits relative to the resonators coupler through the Z-control signals. By changing the energy level crossing points relative to the fixe frequency resonator with the Z-control signals (DC-biased current), we observed the variation of qubit-qubit anti-crossing gap with two-tone spectroscopy on superconducting quantum circuits. Even with the relative noise measurement data in time-domain measurement (without Josephson parameter amplifier and high base-temperature of dilution refrigerator above 25mK), we still can see the variation of envelope of vacuum Rabi oscillation which reflects the change of effective qubit-

qubit coupling. According to the measurement results, the effective qubit-qubit coupling can be tuned from switching off point to two qubit gate point (effective coupling larger than 5 MHz) by just shifting about 50 MHz of qubits' frequencies in double-resonator superconducting quantum circuit.

The paper is organized as follows: In Sec. II, we theoretically analyze the effective qubit-qubit coupling. In Sec. III, the two tone measurement in frequency domian . In Sec. IV, the time-domain measurement of effective qubit-qubit coupling. Finally, we summarize the results in Sec. V.

II. THEORETICAL MODEL

Figure 1 show the sample of double-resonator superconducting quantum circuit, which consist of two tunable Xmon qubits coupling to two common fixed frequency resonators. The resonant frequencies $\omega_{a,b}$ of resonator a,b are fixed, and the transition frequencies $\omega_{1,2}$ of qubit-1,2 can be tuned by the independent Z-control signals. In future multi-qubit chip, the size of resonator coupler can be reduced by using narrower coplanar waveguide resonators to reduce the crosstalks.

According to the previous theoretical work, the second-quantization Hamiltonian of the double resonator coupler superconducting circuit in Fig.1(a) can be written as [13]

$$\begin{aligned}
 H = & \frac{\hbar}{2} \sum_{\lambda=a,b} \omega_{\lambda} c_{\lambda}^{\dagger} c_{\lambda} + \frac{\hbar}{2} \sum_{\beta=1,2} \left(\omega_{\beta} a_{\beta}^{\dagger} a_{\beta} + \alpha_{\beta} a_{\beta}^{\dagger} a_{\beta}^{\dagger} a_{\beta} a_{\beta} \right) \\
 & + \hbar \sum_{\substack{\lambda=a,b \\ \beta=1,2}} g_{\lambda\beta} (c_{\lambda}^{\dagger} a_{\beta} + c_{\lambda} a_{\beta}^{\dagger} - c_{\lambda}^{\dagger} a_{\beta}^{\dagger} - c_{\lambda} a_{\beta}) \\
 & + \hbar g_{ab} (c_a^{\dagger} c_b + c_a c_b^{\dagger} - c_a^{\dagger} c_b^{\dagger} - c_a c_b) \\
 & + \hbar g_{12} (a_1^{\dagger} a_2 + a_1 a_2^{\dagger} - a_1^{\dagger} a_2^{\dagger} - a_1 a_2).
 \end{aligned} \tag{1}$$

The transition frequencies of resonators and qubits are respectively defined as ω_{λ} and ω_{β} , while α_{β} labels the

* wanghuiphy@126.com

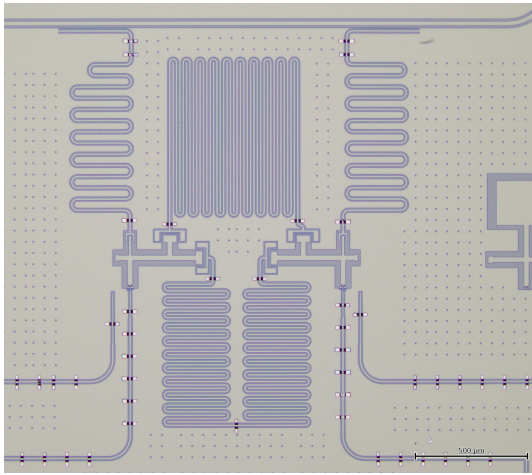


FIG. 1. (Color online) Optical image for Superconducting quantum circuits used in our experiment. The chip consists of two frequency tunable qubits coupling to two common superconducting resonators. The independent XY-control (or Z-control) line is used for microwave-driven (or frequency tuning) of corresponding qubit. The two-body interactions are mainly capacitive types.

anharmonicity of qubit β , with $\lambda = a, b$ and $\beta = 1, 2$. $g_{\lambda\beta}$ is the coupling strength between resonator- λ and qubit- β , while g_{12} (or g_{ab}) describe the directly qubit-qubit (or resonator-resonator) capacitive coupling.

The qubit-resonator coupling strength $g_{\lambda\beta}$ can induce indirect interactions between two qubits, and the effective qubit-qubit coupling strength can be obtained as

$$g_{eff} = \frac{1}{2} \sum_{\lambda=a,b} \left(\frac{g_{\lambda 1} g_{\lambda 2}}{\Delta_{\lambda\beta}} - \frac{g_{\lambda 1} g_{\lambda 2}}{\Sigma_{\lambda\beta}} \right) + g_{12}. \quad (2)$$

Where we have defined $\Delta_{\lambda\beta} = \omega_\beta - \omega_\lambda$ and $\Sigma_{\lambda\beta} = \omega_\beta + \omega_\lambda$. According to Eq.(2), the effective qubit-qubit coupling g_{eff} can be tuned by changing qubits' frequencies ω_β through the flux signals applying from corresponding Z-control lines.

If the transition frequencies of two qubits are tuned between that of two resonator coupler ($\omega_b > \omega_{1,2} > \omega_a$), the high and low frequency resonators will respectively make a negative and positive contributions to the qubit-qubit interaction. When the net contribution of two resonators is same value but opposite sign with the direct qubit-qubit coupling g_{12} , the qubit-qubit coupling can be switched off. Even for extreme small (or even zero) value of g_{12} , the switching off ($g_{12}^{(eff)} = 0$) can be realized without requiring large-scale of frequency shift in the double-resonator coupler superconducting quantum circuit.

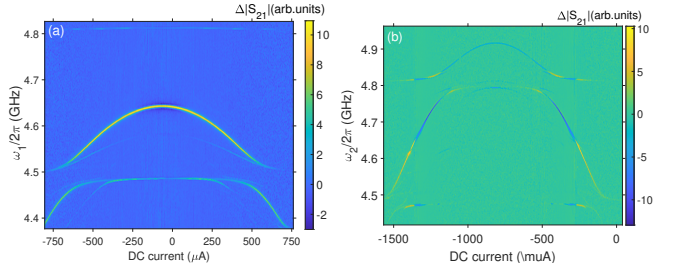


FIG. 2. (Color online) Energy spectrum of qubits under the DC-bias current. The maximal frequency of qubit-1 and qubit-2 are about 4.641 GHz and 4.91 GHz, respectively. Under the strong pumping field, the energy levels of resonator couplers and second-excited states of qubits can also be seen in the energy spectrum. The resonant frequency of low-frequency resonator-a and high-frequency is about 4.47 GHz and 4.80 GHz, respectively. According to corresponding anti-crossing gap, the coupling strength of high (or low)-frequency resonator with qubits are about 30 MHz (or 27 MHz).

III. FREQUENCY DOMAIN MEASUREMENT

The two tone spectroscopy for double-resonator coupler superconducting quantum circuit in Fig.1 are measured with network analyzer (keysight N5231B), microwave source (Agilent E8247c), and two DC-current sources (GS200). With the DC-bias current, according to the energy spectrum in the Fig.2(a), the DC-bias frequency of qubit-1 (qubit-2) is about 4.641 GHz (or 4.691 GHz). Under strong microwave driving field, the energy spectrum of fixed frequency resonator couplers (4.47 GHz and 4.80 GHz) and second-excited states of qubits can also be observed as shown in Fig.2. Since maximal frequency of qubit-1 is between resonant frequencies of two resonator-coupler ($\omega_b > \omega_1^{(max)} > \omega_a$), thus we only see the anti-crossing gap of qubit-1 with resonator-a in Fig.2(a). Since the maximal frequency of qubit-2 is larger than the resonator frequency of two resonator couplers ($\omega_2^{(max)} > \omega_b > \omega_a$), so we can observe the anti-crossing gap of qubit-2 with resonator-a and resonator-b under the DC-bias current as shown in Fig.2(b). The effective coupling of two qubits with the low frequency resonator are about 28 MHz, while 30 MHz with the high frequency resonator according to the measurement energy spectrum or design simulation (qubit-1 and resonator-a).

The transition frequency of qubit-2 is fixed at the certain value by DC-bias current, then the effective qubit-qubit coupling depends on the frequency of qubit-1 (or $\Delta_{\lambda\beta}$) according to Eq.(2). If we apply an independent bias current to sweep the frequency of qubit-1 with DC-biased frequency around transition frequency of qubit-2, then the variation of qubit-qubit anti-crossing gap are shown in Fig.3. By fixing the frequency of qubit-2 at different frequency with DC bias current, and the frequency of qubit-1 sweep around the frequency of qubit-2. The anti-gap reduce from about 10 MHz (4.58 GHz) in Fig.3(a) and reduce to below 2 MHz in Figs.3(d) and

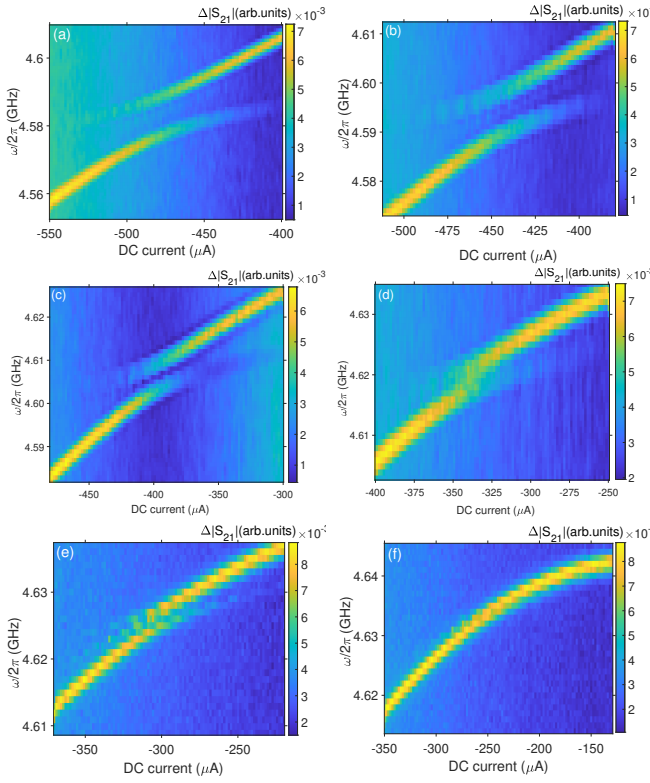


FIG. 3. (Color online) Tunable qubit-qubit anti-crossing gaps. The qubit-2 is fixed at 6 different frequencies, and the anti-crossing gap are measured by sweeping the frequency of qubit-1 (with the DC-biased current) around the corresponding frequency of qubit-2 as shown in (a)-(f).

3(e) (close to 4.62 GHz). If qubit-2 is tuned to about 4.37 GHz, the anti-crossing gap is almost invisible in Fig.3(e) where the qubit-qubit coupling is turned off. By choosing direct qubit-qubit coupling as 0.88 MHz, with the qubit-resonator coupling strength obtained from the anti-crossing gap, the calculated switching off point coincide well the measurement results in Fig.(3).

By only shifting 50 MHz from the switching off points with flux pulse, the anti-crossing gap effective qubit-qubit coupling can be tuned from 0 Hz to about 5 MHz as shown in Fig.3(a). Thus the switching off positions can be very close to two-qubit gate regimes (about 5 MHz effective qubit-qubit coupling), thus the flux noises can be greatly suppressed during the quantum operations for the double-resonator couplers superconducting quantum chip. The double-resonators coupler can turn off the qubit-qubit coupling without requiring additional flux lines, this can reduce flux noises and the occupation number for high-frequency cables of dilution refrigerator.

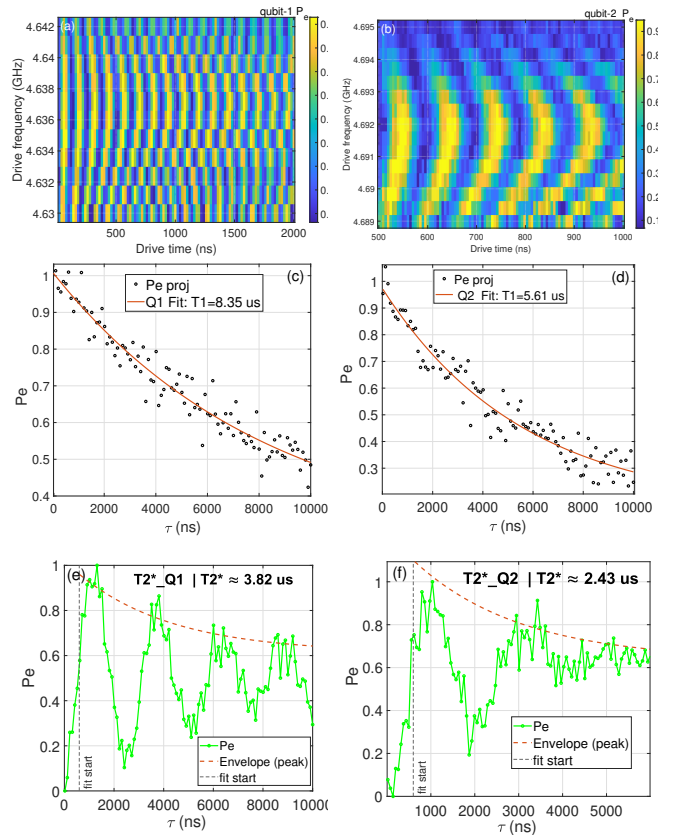


FIG. 4. (Color online) (a) Rabi oscillation of two qubits under the DC-bias current (no flux pulse). The center frequencies of two Rabi oscillation under are respectively $\omega_1^{(bias)}/2\pi = 4.637$ GHz and $\omega_2^{(bias)}/2\pi = 4.691$ GHz. The T_1 (or T_2) are respectably measured in (c) (or (e)) at 4.637 GHz for qubit-1 and (d) (or (f)) at 4.692 GHz for qubit-2.

IV. TIME-DOMAIN MEASUREMENT

The vacuum Rabi oscillation period can also reflect effective qubit-qubit coupling strength between two qubits[15, 25]. To avoid level crossing between qubit-2 and high-frequency resonator in the vacuum Rabi experiment, we tune qubit-2 (or qubit-1) to 4.691 GHz (or 4.637 GHz) with the DC-bias currents. DC-Biased Frequencies of two qubits are close to the switching off points (around 4.637 GHz as indicated by Fig.2), this can reduce signal distortions (at large pulse amplitude) in the vacuum Rabi measurement. In the case of zero flux pulse, the Rabi oscillation of two qubits are measured as shown in Figs.4(a) and 4(b). In the absent of flux pulse, the coherent time T_1 and T_2 for two qubits are measured in Figs.4(c)-4(f) where the frequency detuning is about 50 MHz during the T_1 and T_2 measurement. The large fluctuations on the curves of T_1 and T_2 indicate the low readout Signal-to-Noise Ratio (without Josephson parameter amplifier) and relative high base temperature (above 25 mK) of dilution refrigerator. In the regimes of strong flux pulses,

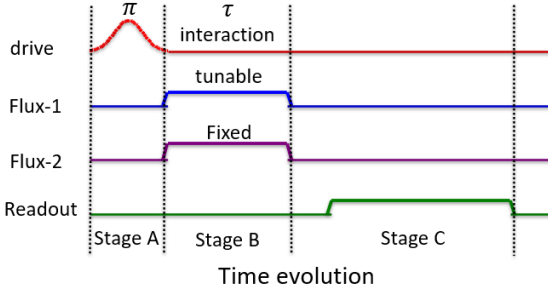


FIG. 5. (Color online) Pulse sequence employed for the Vacuum Rabi measurement. In the stage A, the π pulse drive qubit-2 to its first-excited state. In the stage B, the flux pulse-2 tune the qubit-2 to 4.637 GHz, simultaneously qubit-1 is tuned close to 4.637 GHz with the flux pulse-1. The two qubits interaction interval (τ) is decided by simultaneous holding period of two flux pulses in stage-B. After the interaction finished, two flux pulse turned off, and the quantum states of qubit-1 will be readout in stage C (at frequency 4.637 GHz). The time interval between driving π -pulse and readout pulse fixes at a certain value (within the coherent times of two qubits.)

the Rabi response spectrum (phase) curve of qubit will be divergent as shown in Fig.8 (see Appendix).

Pulse sequences employed for vacuum Rabi measurement are shown in Fig.5. In stage-A, the π pulse drive qubit-2 to its first-excited state in the case of zero flux pulse (4.691 GHz) which reduce the frequency drift induced by the flux pulse distortion[4, 20, 21]. Immediately after π pulse exciting qubit-2 to its first excited states, the flux pulse-2 will tune qubit-2 to 4.637 GHz in stage-B, and simultaneously flux pulse-1 shift qubit-1 close to 4.637 GHz. The two near resonant qubits will exchange energy with each other in state-B, then one dimensional vacuum Rabi curve can be plotted as the function of interaction duration τ as shown in Fig.6. The amplitude of flux pulse-1 is tunable to sweep the transition frequency of qubit-1, and then we can measure a series of Vacuum Rabi curves at different qubit-qubit frequency detuning. After the interaction finished(roughly stage-B), the qubits will return to the DC-biased frequency after zero the amplitudes of two flux pulse, then we read the occupation probabilities of qubit-1. To reduce the signal drift, the time interval between driving π -pulse and readout pulse fix at a certain value (about 1.2us) smaller than the coherent times of two qubits.

For the vacuum Rabi oscillation measurement, the qubit-1 exchange energy with qubit-2 through near resonant interactions, then the occupation probabilities of qubit-1 with interaction time duration[15, 25] In the case of two qubits near resonant, the maximal occupation probability should be $P_{1,max} \sim \exp(-T_{swap}/T_2)$, while $T_{swap} = \pi/2|g_{eff}|$. As indicated by the small anti-crossing gaps in Fig.2, the effective qubit-qubit coupling is quite weak close to the switching off point. If

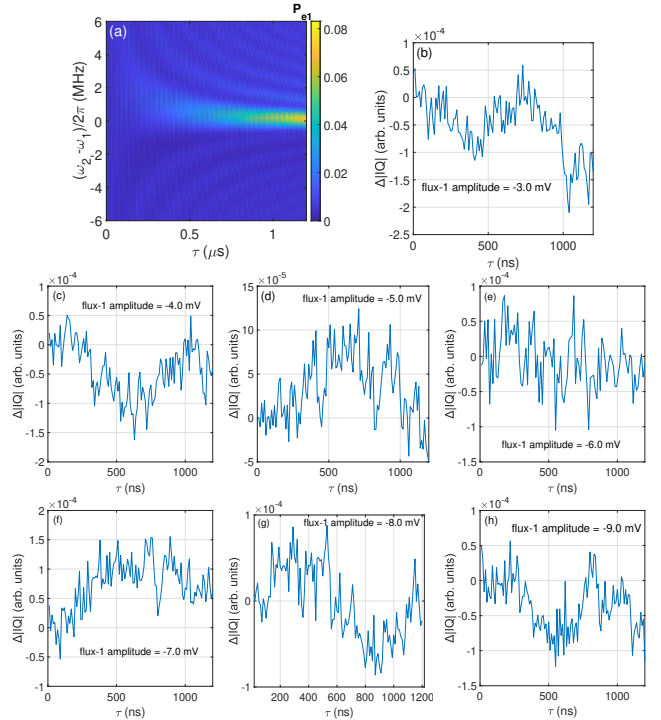


FIG. 6. (Color online) Vacuum Rabi oscillation. (a) Simulation of Vacuum Rabi oscillation. The occupation probabilities of qubit-1 as the function of interaction time and frequency detuning between two qubits. (b)-(h) Readout contrast relative to the ground-state baseline ($|IQ| - \text{baseline}$) at different frequency detuning between two qubits. The pulse amplitude for qubit-1 vary in (b)-(h), and the flux-1 amplitude =:(b)-3 mV;(c)-4 mV;(d)-5 mV;(e)-6 mV; (f)-7 mV; (g) -8 mV; (g)-9 mV.

two qubits are in the off-resonant case, the maximal occupation probabilities of qubit-1 first excited-state is $P_{1,max} = 4g_{eff}^2/(\Delta_{12}^2 + 4g_{eff}^2)$ which is usually smaller than one, with $\Delta_{12} = \omega_2 - \omega_1$. Since T_{swap} is close and even larger than T_2 in this measurement, thus the maximal occupation probabilities for qubit-1 can be much smaller than one as indicated by the simulation result with the lindblad master equation (see Fig.6(a))[23, 24].

In the absence of Josephson parameter amplifier and the relative high base temperature (above 25mK), the Signal-to-Noise Ratio is not high in this measurement. If we use the normalization method to calculate excited state occupation probabilities, more errors will be induced by the noise data. As shown in Figs.6(b)-6(h), we use $\Delta|IQ| (= |IQ| - \text{baseline})$ to describe the variation of the readout signal which can reflect envelope variations of vacuum Rabi oscillation. Even with low SNR, we still can see some feature of envelope variation of $\Delta|IQ|$ from the noisy data (see Figs.6(b)-6(h)). When the flux pulse amplitude is close to -6.0 mV, the envelope of $\Delta|IQ|$ is not clear in Fig.6(e), which should be close to switching off point(see fig.3). As the change of the flux pulse amplitude of qubit-1, the envelope for the curve of $\Delta|IQ|$ become clearer at larger frequency detuning ($|\Delta_{12}|$) because

of nonzero energy exchange between two qubits, the oscillation periods of $\Delta|IQ|$ reflect variation of qubit-qubit coupling strength. The switching off point measured by the Vacuum Rabi oscillation roughly coincide with the anti-crossing gap in the frequency domain. The measurement result should be enhanced in future experiment if we add the Josephson parameter amplifier, Purcell filter, and enhance the effective qubit-qubit coupling.

V. CONCLUSIONS

In conclusion, we experimentally studied tunable qubit-qubit coupling in the double-resonator coupler type superconducting quantum circuit. The induced indirect qubit-qubit coupling by two resonators can be cancelled, so the switching off can be realized without the direct qubit-qubit coupling. In the frequency domain and time-domain, we observed the variation of the effective qubit-qubit induced by the two-fixed frequency resonators. In future experiment, we will add the Josephson parameter amplifier, Purcell filter, and also conduct the calibration of Z-pulse distortion to improve the measurement result.

VI. ACKNOWLEDGMENTS

Hui Wang thank Zhiguang Yan for valuable suggestions on the hardware setup, measurement codes writing, and measurement result analysis. We also thank Shiyu Wang and Russell S. Deacon for friendly help during the measurement and fabrication of the samples, and also Chih-Yao Shih, Ching-Yeh Chen, Hiroto Mukai, and Hang Xue for maintaining the running of dilution refrigerator. J.S. Tsai is supported by the Japan Science and Technology Agency (Moonshot R D, JPMJMS2067; CREST, JPMJCR1676) and the New Energy and Industrial Technology Development Organization (NEDO, JPNP16007).

APPENDIX A: THE NUMERICAL CALCULATION OF THE ENERGY LEVELS

A. Experiment setup

The measurement is use the keysight M3202A and digitizer M3102A, the microwave signals are created by the RS sgs100a. The attenuation in the read-in and XY control line are about 60db, and about 44db for the Z-control line. The DC-current and the flux pulse is combined by the bias-Tee in room temperature. The infrared filter are

installed for the driving and readout cable. The DC current will bias the qubits at suitable frequency points for the Rabi or the vacuum Rabi measurement, while the flux pulse is for the fast sweeping of qubits' frequency, and

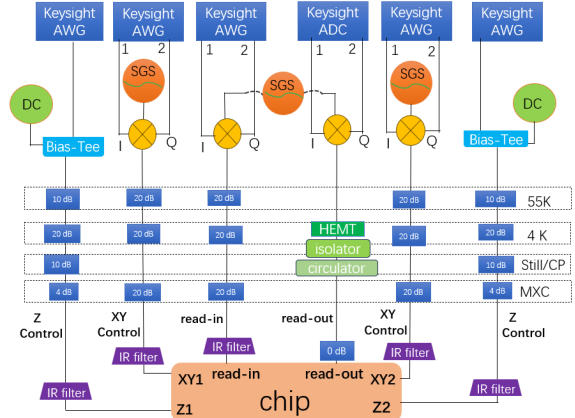


FIG. 7. (Color online) Electronics and sample schematic diagram for the vacuum rabi measurement.

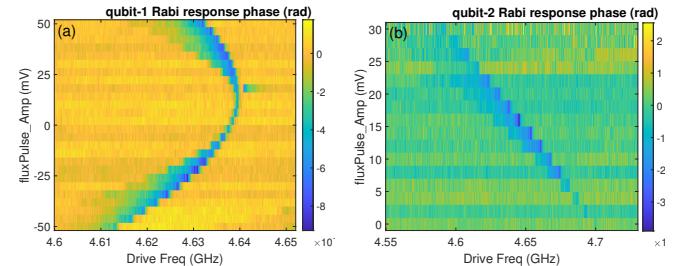


FIG. 8. (Color online) The Rabi response spectrum (phase). Rabi response spectrums (phase) for (a) qubit-1 and (b) qubit-2 under the flux pulses. The zero flux correspond to the DC-bias frequencies of two qubits. Rabi response spectrums become divergent at large pulse amplitude because of Z-pulse distortion.

they combined together with each other in room temperature with a bias-Tee.

B. Rabi-frequency spectrum under flux-pulse

Close to the DC-bias frequency of qubit-1 (qubit-2) at 4.691 GHz (or 4.637 GHz), the Rabi response spectrum of two qubits can be measured by applying corresponding flux pulses are shown in Fig.8. The energy spectrum curves of two qubit become divergent at large amplitude of flux pulse because of Z pulse distortion[4, 20, 21]. We did not calibrate the Z-pulse distortion in this experiment, and the vacuum Rabi measurement will focus on the parameter regimes close to 4.637 GHz where the Z-pulse distortion is small because of small flux pulse amplitudes.

[1] Y. Chen, C. Neill, P. Roushan, N. Leung, M. Fang, R. Barends, J. Kelly, B. Campbell, Z. Chen, B. Chiaro, A. Dunsworth, E. Jeffrey, A. Megrant, J. Y. Mutus, P. J. J. ÓMalley, C. M. Quintana, D. Sank, A. Vainsencher, J. Wenner, T. C. White, Michael R. Geller, A. N. Cleland, and J. M. Martinis, qubit Architecture with High Coherence and Fast Tunable Coupling, *Phys. Rev. Lett.* 113, 220502 (2014).

[2] X. Li, T. Cai, H. Yan, Z. Wang, X. Pan, Y. Ma, W. Cai, J. Han, Z. Hua, X. Han, Y. Wu, H. Zhang, H. Wang, Yipu Song, Luming Duan, and Luyan Sun, Tunable Coupler for Realizing a Controlled-Phase Gate with Dynamically Decoupled Regime in a Superconducting Circuit, *Phys. Rev. Appl.* 14, 024070 (2020).

[3] Yuan Xu, Ji Chu, Jiahao Yuan, Jiawei Qiu, Yuxuan Zhou, Libo Zhang, Xinshe Tan, Yang Yu, Song Liu, Jian Li, Fei Yan, and Dapeng Yu, High-Fidelity, High-Scalability Two-Qubit Gate Scheme for Superconducting Qubits, *Phys. Rev. Lett.* 125, 240503 (2020).

[4] F. Yan, P. Krantz, Y. Sung, M. Kjaergaard, D. L. Campbell, T. P. Orlando, S. Gustavsson, and W. D. Oliver, Tunable Coupling Scheme for Implementing High-Fidelity Two-qubit Gates, *Phys. Rev. Appl.* 10, 054062 (2018).

[5] F. Arute, K. Arya, R. Babbush, D. Bacon, J. C. Bardin, R. Barends, R. Biswas, S. Boixo, F. G. S. L. Brandao, D. A. Buell, B. Burkett, Yu Chen, Zijun Chen, B. Chiaro, R. Collins, W. Courtney, A. Dunsworth, E. Farhi, B. Foxen, A. Fowler, C. Gidney, M. Giustina, R. Graff, K. Guerin, S. Habegger, M. P. Harrigan, M. J. Hartmann, A. Ho, M. Hoffmann, T. Huang, T. S. Humble, S. V. Isakov, E. Jeffrey, Zhang Jiang, D. Kafri, K. Kechedzhi, Julian Kelly, P. V. Klimov, S. Knysh, A. Korotkov, F. Kostritsa, D. Landhuis, M. Lindmark, E. Lucero, D. Lyakh, S. Mandrà, J. R. McClean, M. McEwen, A. Megrant, Xiao Mi, K. Michielsen, M. Mohseni, J. Mutus, O. Naaman, M. Neeley, C. Neill, M. Y. Niu, E. Ostby, A. Petukhov, J. C. Platt, C. Quintana, E. G. Rieffel, P. Roushan, N. C. Rubin, D. Sank, K. J. Satzinger, V. Smelyanskiy, K. J. Sung, M. D. Trevithick, A. Vainsencher, B. Villalonga, T. White, Z. J. Yao, P. Yeh, A. Zalcman, H. Neven, J. M. Martinis, Quantum supremacy using a programmable superconducting processor, *Nature* 574, 505 (2019).

[6] Yulin Wu, Wan-Su Bao, Sirui Cao, Fusheng Chen, Ming-Cheng Chen, Xiawei Chen, Tung-Hsun Chung, Hui Deng, Yajie Du, Daojin Fan, Ming Gong, Cheng Guo, Chu Guo, Shaojun Guo, Lianchen Han, Linyin Hong, He-Liang Huang, Yong-Heng Huo, Liping Li, Na Li, Shaowei Li, Yuan Li, Futian Liang, Chun Lin, Jin Lin, Haoran Qian, Dan Qiao, Hao Rong, Hong Su, Lihua Sun, Liangyuan Wang, Shiyu Wang, Dachao Wu, Yu Xu, Kai Yan, Weifeng Yang, Yang Yang, Yangsen Ye, Jiahnan Yin, Chong Ying, Jiale Yu, Chen Zha, Cha Zhang, Haibin Zhang, Kaili Zhang, Yiming Zhang, Han Zhao, Youwei Zhao, Liang Zhou, Qingling Zhu, Chao-Yang Lu, Cheng-Zhi Peng, Xiaobo Zhu, and Jian-Wei Pan, Strong Quantum Computational Advantage Using a Superconducting Quantum Processor, *Phys. Rev. Lett.* 127, 180501 (2021).

[7] Y. Sung, L. Ding, J. Braumüller, A. Vepsäläinen, B. Kannan, M. Kjaergaard, A. Greene, G. O. Samach, C. McNally, D. Kim, A. Melville, B. M. Niedzielski, M. E. Schwartz, J. L. Yoder, T. P. Orlando, S. Gustavsson, and W. D. Oliver, Realization of High-Fidelity CZ and ZZ-Free ISWAP Gates with a Tunable Coupler, *Phys. Rev. X* 11, 021058 (2021).

[8] I.N. Moskalenko, I.A. Simakov, N.N. Abramov, A.A. Grigorev, D.O. Moskalev, A.A. Pishchimova, N.S. Smirnov, E.V. Zikiy, I.A. Rodionov, and I.S. Besedin, High fidelity two-qubit gates on fluxoniums using a tunable coupler, *Npj Quantum Inform.* 8, 130 (2022).

[9] Acharya et al. — Quantum error correction below the surface code threshold, *Nature* 638, 920–926 (2025)

[10] N. Lacroix et al. (Google Quantum AI), Scaling and logic in the colour code on a superconducting processor, *Nature* volume 645, pages614–619 (2025).

[11] Tan et al, Experimental Quantum Error Correction below the Surface Code Threshold via All-Microwave Leakage Suppression, *Phys. Rev. Lett.* 135, 260601 – Published 22 December, (2025).

[12] Ming Gong, Shiyu Wang, Chen Zha, Ming-Cheng Chen, He-Liang Huang, Yulin Wu, Qingling Zhu, Youwei Zhao, Shaowei Li, Shaojun Guo, Haoran Qian, Yangsen Ye, Fusheng Chen, Chong Ying, Jiale Yu, Daojin Fan, Dachao Wu, Hong Su, Hui Deng, Hao Rong, Kaili Zhang, Sirui Cao, Jin Lin, Yu Xu, Lihua Sun, Cheng Guo, Na Li, Futian Liang, V. M. Bastidas, Kae Nemoto, W. J. Munro, Yong-Heng Huo, Chao-Yang Lu, Cheng-Zhi Peng, Xiaobo Zhu, Jian-Wei Pan, Quantum walks on a programmable two-dimensional 62-qubit superconducting processor, *Science* 372, 948(2021).

[13] Hui Wang, Yan-Jun Zhao, Hui-Chen Sun, Xun-Wei Xu, Yong Li, Yarui Zheng, Qiang Liu, and Rengang Li, Controlling the qubit-qubit coupling in the superconducting circuit with double-resonator couplers, *Physical review A* 109, 012601 (2024).

[14] IBM-Q-Team, IBM-Q-53 Rochester backend specification v1.2.0, (2020).

[15] Yulin Wu, Li-Ping Yang, Ming Gong, Yarui Zheng, Hui Deng, Zhiguang Yan, Yanjun Zhao, Keqiang Huang, A. D Castellano, W. J Munro, K. Nemoto, Dong-Ning Zheng, C.P. Sun, Yu-xi Liu, Xiaobo Zhu, Li Lu, An efficient and compact switch for quantum circuits, *npj Quantum Inf.* 4, 50 (2018).

[16] J. Stehlik, D.M. Zajac, D.L. Underwood, T. Phung, J. Blair, S. Carnevale, D. Klaus, G.A. Keefe, A. Carniol, M. Kumph, M. Steffen, and O.E. Dial, Tunable Coupling Architecture for Fixed-Frequency Transmon Superconducting Qubits, *Phys. Rev. Lett.* 127, 080505 (2021).

[17] D.C. McKay, S. Filipp, A. Mezzacapo, E. Magesan, J.M. Chow, and J.M. Gambetta, Universal Gate for Fixed-Frequency Qubits via a Tunable Bus, *Phys. Rev. Appl.* 6, 064007(2016).

[18] Hui Wang, Yan-Jun Zhao, Rui Wang, Xun-Wei Xu, Qiang Liu, Jianhua Wang, and Changxin Jin, Frequency Adjustable Resonator as a Tunable Coupler for Xmon Qubits, *J. Phys. Soc. Jpn.* 91, 104005 (2022).

[19] Z. Yan, Y.-R. Zhang, M. Gong, Y. Wu, Y. Zheng, S. Li, C. Wang, F. Liang, J. Lin, Y. Xu, C. Guo, L. Sun, C.-Z. Peng, K. Xia, H. Deng, H. Rong, J. Q. You, F. Nori, H. Fan, X. Zhu, and J.-W. Pan, Strongly correlated quantum walks with a 12-qubit superconducting processor,

Science 364, 753 (2019).

[20] Rui Li, Kentaro Kubo, Yinghao Ho, Zhiguang Yan, Yasunobu Nakamura, and Hayato Goto, Realization of High-Fidelity CZ Gate Based on a Double-Transmon Coupler, Phys. Rev. X 14, 041050 (2024).

[21] Tian-Ming Li, Jia-Chi Zhang, Bing-Jie Chen, Kaixuan Huang, Hao-Tian Liu, Yong-Xi Xiao, Cheng-Lin Deng, Gui-Han Liang, Chi-Tong Chen, Yu Liu, Hao Li, Zhen-Ting Bao, Kui Zhao, Yueshan Xu, Li Li, Yang He, Zheng-He Liu, Yi-Han Yu, Si-Yun Zhou, Yan-Jun Liu, Xiaohui Song, Dongning Zheng, Zhong-Cheng Xiang, Yun-Hao Shi, Kai Xu, Heng Fan, High-precision pulse calibration of tunable couplers for high-fidelity two-qubit gates in superconducting quantum processors, Phys. Rev. Applied. 23, 024059 (2025).

[22] Hayato Goto, Double-Transmon Coupler: Fast Two-Qubit Gate with No Residual Coupling for Highly Detuned Superconducting Qubits, Phys. Rev. Appl. 18, 034038 (2022).

[23] J. R. Johansson, P. D. Nation, and F. Nori: "QuTiP 2: A Python framework for the dynamics of open quantum systems.", Comp. Phys. Comm. 184, 1234 (2013) [DOI: 10.1016/j.cpc.2012.11.019].

[24] J. R. Johansson, P. D. Nation, and F. Nori: "QuTiP: An open-source Python framework for the dynamics of open quantum systems.", Comp. Phys. Comm. 183, 1760 (2012) [DOI: 10.1016/j.cpc.2012.02.021].

[25] Gui-Han Liang, Xiao-Hui Song, Cheng-Lin Deng, Xu-Yang Gu, Yu Yan, Zheng-Yang Mei, Si-Lu Zhao, Yi-Zhou Bu, Yong-Xi Xiao, Yi-Han Yu, Ming-Chuan Wang, Tong Liu, Yun-Hao Shi, He Zhang, Xiang Li, Li Li, Jing-Zhe Wang, Ye Tian, Shi-Ping Zhao, Kai Xu, Heng Fan, Zhong-Cheng Xiang, Dong-Ning Zheng, Tunable-coupling architectures with capacitively connecting pads for large-scale superconducting multiqubit processors, Phys. Rev. Applied 20, 044028 (2023).